# Retrieval of electron-atom scattering cross sections from laser-induced electron rescattering of atomic negative ions in intense laser fields

XiaoXin Zhou,[1,2] Zhangjin Chen,[1] Toru Morishita,[1,3] Anh-Thu Le,[1] and C. D. Lin[1]

[1]*J. R. Macdonald Laboratory, Physics Department, Kansas State University, Manhattan, Kansas 66506-2604, USA*
[2]*College of Physics and Electronic Engineering, Northwest Normal University, Lanzhou 730070, People's Republic of China*
[3]*Department of Applied Physics and Chemistry, University of Electro-Communications, Tokyo, 182-8585, Japan*
*and PRESTO, Japan Science and Technology Agency, Kawaguchi, Saitama, 332-0012, Japan*

We investigated the two-dimensional electron momentum distributions of atomic negative ions in an intense laser field by solving the time-dependent Schrödinger equation (TDSE) and using the first- and second-order strong-field approximations (SFAs). We showed that photoelectron energy spectra and low-energy photoelectron momentum distributions predicted from SFAs are in reasonable agreement with the solutions from the TDSE. More importantly, we showed that accurate electron-atom elastic scattering cross sections can be retrieved directly from high-energy electron momentum spectra of atomic negative ions in the laser field. This opens up the possibility of measuring electron-atom and electron-molecule scattering cross sections from the photodetachment of atomic and molecular negative ions by intense short lasers, respectively, with temporal resolutions in the order of femtoseconds.

PACS number(s): 32.80.Rm, 32.80.Gc, 42.50.Hz

## I. INTRODUCTION

In the past two decades, the energy and momentum spectra of electrons generated by the ionization of atoms or detachment of negative ions by intense laser pulses have been widely investigated [1,2]. In particular, the detachments of negative hydrogen and fluorine ions in intense laser fields have been reported in experiments [3–7] and in theory [8–15], using either the strong-field approximation (SFA) or by solving the time-dependent Schrödinger equation (TDSE). These studies have shown that experimentally observed spectra are largely well reproduced by theoretical calculations. However, the electrons measured in these experiments tend to be restricted to low energies, and SFA and TDSE calculations are often carried out by separate groups.

In this paper, we studied the photodetachment of H⁻ and F⁻ negative ions in short intense laser pulses. Our goal is to examine the electron energy spectra and two-dimensional (2D) electron momentum distributions over a broad energy range, from the threshold up to 10 $U_p$, where $U_p$ is the ponderomotive energy—the kinetic energy of a classical quivering electron in the laser field, averaged over a laser cycle. We will use the standard first-order SFA (SFA1) and the second-order SFA (SFA2) to describe the photodetachment process, as well as obtaining the same spectra by solving the TDSE directly. The negative ion will be approximated by a model potential and the same potential is used in the SFA and TDSE calculations. We will establish, based on specific numerical results, the accuracy of the SFA for describing the photodetachment of negative ions by lasers. In SFA, it was assumed that electrons released into the continuum can be described as a free electron in the laser field, and that there are no excited states in the target atom. Both approximations are expected to work better for negative ion targets than for atomic targets. Indeed our calculations showed that the total electron energy spectra and the electron momentum distributions at low energies calculated from the SFA are in quite

good overall agreement with the TDSE results, to within about a factor of 2. Such agreement has not been seen if the targets are neutral atoms or positive ions [16]. Our major goal, however, is to establish that high-energy electron momentum spectra of negative ions induced by intense short laser pulses can be used to extract the elastic differential cross sections of neutral atoms by free electrons. Similar conclusions have been shown recently for atoms where electron-ion scattering cross sections can be extracted from laser-induced high-energy electron momentum spectra of neutral atoms [17].

In Sec. II, we summarize the theoretical models used. The numerical results for H⁻ and F⁻ from SFA and TDSE are presented and analyzed in Sec. III, for both the energy distributions and the 2D momentum distributions. From the high-energy 2D photoelectron momentum distributions we will extract the *e*-H and *e*-F elastic scattering cross sections. In Section IV we summarize the results and discuss the important possible applications of using laser-induced photoelectron spectra for probing time-resolved electron-atom or electron-molecule collisions. Atomic units are used throughout, unless otherwise indicated.

## II. THEORETICAL METHODS

We will model each negative ion in the single-active electron (SAE) approximation. In this model, the time-dependent wave function of the active electron in the laser field is governed by

$$i\frac{\partial}{\partial t}\psi(\mathbf{r},t) = [H_0 + H'(t)]\psi(\mathbf{r},t),\tag{1}$$

where $H_0 = -\frac{1}{2}\nabla^2 + V(\mathbf{r})$ is the electron Hamiltonian of the laser-free system, with $V(\mathbf{r})$ being the atomic model potential, and $H'(t) = \mathbf{r} \cdot \mathbf{E}(t)$ is the interaction of the electron with the laser's electric field $\mathbf{E}(t)$. Equation (1) can be solved

numerically by using the split-operator method [18,19]. The electron momentum spectra are obtained by projecting out the final time-dependent wave function after the laser pulse is over using the continuum scattering eigenstates of the laser-free Hamiltonian. For electrons with momentum $p$ in the direction $\hat{\mathbf{p}}$, with respect to the laser polarization direction, if the detachment amplitude is $f$, then the angular distributions at energy $E = p^2/2$ is given by

$$\frac{\partial P}{\partial \mathbf{p}} = |f(\mathbf{p})|^2. \tag{2}$$

By integrating over the directions of photoelectrons at a fixed energy $E$, the energy dependence of the photoelectrons are calculated from

$$\frac{\partial P}{\partial E} = \int |f(\mathbf{p})|^2 p \, d\hat{\mathbf{p}}. \tag{3}$$

In the strong-field approximation, the detachment amplitude of electrons with momentum $\mathbf{p}$ is expressed as [22]

$$f(\mathbf{p}) = f^{(1)} + f^{(2)}, \tag{4}$$

where the SFA1 amplitude is

$$f^{(1)} = -i \int_{-\infty}^{\infty} dt \langle \chi_{\mathbf{p}}(t) | H'(t) | \Psi_0(t) \rangle \tag{5}$$

and the SFA2 amplitude is

$$f^{(2)} = - \int_{-\infty}^{\infty} dt \int_{-\infty}^{t} dt' \int d\mathbf{k} \langle \chi_{\mathbf{p}}(t) | V | \chi_{\mathbf{k}}(t) \rangle$$
$$\times \langle \chi_{\mathbf{k}}(t') | H'(t') | \Psi_0(t') \rangle. \tag{6}$$

Here $\chi_{\mathbf{p}}(t)$ and $\Psi_0(t)$ are the Volkov states of a continuum electron with momentum $\mathbf{p}$ and the initial state, respectively. Note that there are different versions of formulating the SFA2 [20,21]. Our version follows the work of Milošević *et al.* [9]. The evaluation of the integral (6) has been discussed in Ref. [22]. In SFA2, we have used the saddle point approximation in evaluating the integration over $d\mathbf{k}$ where $\mathbf{k}$ is the momentum of photoelectron in the intermediate Volkov state. The procedure is similar to what was used in Lewenstein *et al.* [23]. The result of saddle point integration for the fivefold integral (6) is obtained by setting

$$\mathbf{k} = -\frac{1}{t - t'} \int_{t'}^{t} dt'' \mathbf{A}(t'') \tag{7}$$

and substituting

$$\int d\mathbf{k} \rightarrow \left[ \frac{2\pi}{\epsilon + i(t - t')} \right]^{3/2} \tag{8}$$

for the integration over $\mathbf{k}$. When $t \rightarrow t'$, the integral (6) converges for the case of initial state $\Psi_0$ having $S$ symmetry (as for H$^-$), while it is divergent for the case of $P$ symmetry (as for F$^-$). In general, an "arbitrary" small parameter $\epsilon$ is introduced in Eq. (8) to avoid possible divergence of the integral when $t \rightarrow t'$. It has been verified numerically that, for the case of H$^-$, the SFA2 amplitude does not change for $\epsilon$ in the

range of 0.01 to 0.5. Therefore, the magnitude of SFA2 for H$^-$ in the present work is absolute. This situation is different for neutral atomic targets. In order to evaluate SFA2, another damping parameter has to be introduced into the long-range Coulomb potential to avoid the singularity [22]. This damping factor does affect the magnitude of the SFA2 amplitude but not the shape of the photoelectron energy and the 2D momentum spectra in the high-energy region [22]. Since the magnitude of SFA1 for neutral atomic target is also grossly incorrect, for neutral targets the SFA1 and SFA2 are used only to examine their predictions of the energy and momentum dependence, in the low- and high-energy region, respectively, see Ref. [22].

It should be noted that, for F$^-$ with initial state of $P$-symmetry, the SFA2 amplitude does depend on $\epsilon$ in Eq. (8). For a wavelength of 1800 nm laser pulse considered for F$^-$ in this paper, it has been found that the SFA2 energy spectra above $4U_p$ remain the same when $\epsilon$ varies from 0.1 to 1.0 while the energy spectra below $1U_p$ change about 10 times. In our numerical calculations, we choose $\epsilon = T/500$ (about 0.5), where $T$ is the period of the laser.

The model potential for H$^-$ is taken from Ref. [24]:

$$V(r) = -\left(1 + \frac{1}{r}\right)e^{-2r} - \frac{\alpha_d}{2r^4}(1 - e^{(r/r_c)^6}) + V_0(r), \tag{9}$$

where $V_0(r) = (c_0 + c_1 r + c_2 r^2)e^{-\beta r}$. Note that the polarization of the core (H atom) has been included in Eq. (9), with $\alpha_d$ and $r_c$ being the polarizability and the cutoff constant, respectively. The parameters in Eq. (9) are listed in Ref. [24].

For F$^-$, we chose the potential to have the form

$$V(r) = -a_1 \frac{e^{-\alpha_1 r}}{r} - a_2 \frac{e^{-\alpha_2 r}}{r}. \tag{10}$$

From fitting, the parameters $a_1$, $a_2$, $\alpha_1$, and $\alpha_2$ obtained are 5.137, 3.863, 1.288, and 3.545, respectively. This potential gives the correct ground-state energy, and its lowest $p$-orbital eigenfunction agrees well with the tabulated Hartree-Fock wave function for F$^-$.

## III. RESULTS AND DISCUSSION

We used the TDSE and SFA to calculate the energy spectra and the 2D momentum distributions of H$^-$ and F$^-$ in intense laser fields. For H$^-$, we took peak laser intensity of $I = 1.0 \times 10^{11}$ W/cm$^2$, wavelength $\lambda = 10\,600$ nm and pulse duration of three cycles. The electric field has the form $E(t) = E_0 F(t) \cos(\omega t + \phi)$, where $\phi$ (we chose it to be zero) is the carrier envelope phase and $F(t) = \cos^2(\pi t/\tau)$, where $\tau = 3T$ ($|t| \leq \tau/2$). For this laser pulse $U_p = 1.05$ eV and it needs 16 photons ($\hbar\omega = 0.117$ eV) to remove the electron from H$^-$. The Keldysh parameter is 0.6, thus the electron detachment is well in the tunneling regime.

In Fig. 1 we show the photoelectron energy spectra in terms of $U_p$. In the SFA, the low-energy part below about $3.5U_p$ is dominated by SFA1, while the yield above $4U_p$ is dominated almost entirely by SFA2, i.e., it is due to the recollision between the detached electrons with the neutral target H. The figure also shows that the energy spectra ob-
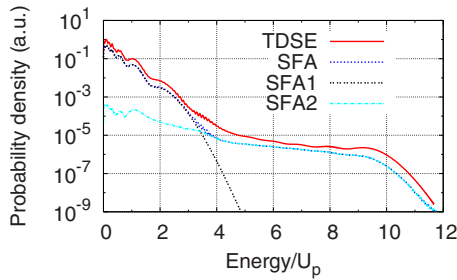
FIG. 1. (Color online) Energy spectra of laser-induced photo-electrons of H$^-$ obtained from TDSE and SFA. The laser parameters are $I=1.0\times10^{11}$ W/cm$^2$ and $\lambda=10\,600$ nm for a pulse with three optical cycles (see text).

tained from SFA are only about a factor of 2 smaller than those obtained from the TDSE. For neutral atom or positive ion targets the absolute total ionization yields calculated using SFA are generally much smaller, close to one order or more smaller than those obtained from TDSE [16].

Figure 2 shows the 2D momentum distributions of the detached electrons at low energies, where $p_\parallel$ refers to the direction of the laser polarization and $p_\perp = \sqrt{p^2 - p_\parallel^2}$ is perpendicular to it. Here we have normalized the data to the same peak value in the two graphs. There are several special features that should be mentioned. First, the 2D spectra predicted from SFA1 and from TDSE are very close to each other. Second, the low-energy 2D electron spectra exhibit clean structures that are similar to multiphoton detachment (MPD) spectra, despite the fact that the the laser-ion interaction is in the tunneling regime. It is interesting to compare these low-energy 2D momentum spectra with those from neutral atomic targets [18]. To begin with, for atomic targets, the low-energy momentum spectra show fanlike structure emanating from the origin. These fanlike structures have been observed experimentally [25,26], and are seen only from the TDSE calculations, not from the SFA1 calculations. The fanlike structures had been attributed to the long-range Coulomb interaction between the electron and the positive
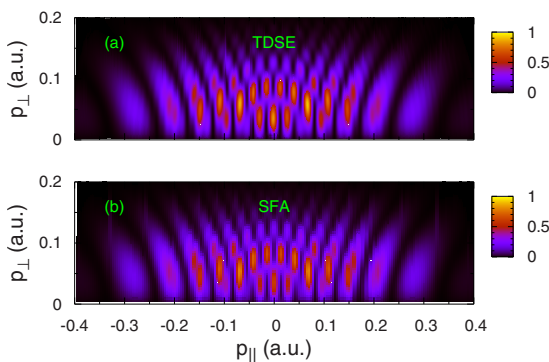


FIG. 2. (Color online) 2D momentum distributions of laser-induced photoelectrons of H$^-$ in the low-energy region, obtained from TDSE (a) and from SFA (b). The horizontal axis is the electron momentum along the direction of laser polarization and the vertical axis is any axis perpendicular to it (the electron spectrum has cylindrical symmetry.) The laser parameters are the same as in Fig. 1.
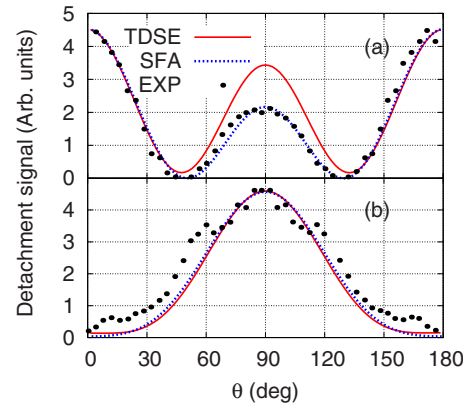


FIG. 3. (Color online) Angular distributions of laser-induced photoelectrons of H$^-$, generated by a laser with wavelength $\lambda=2150$ nm. (a) Intensity $I=1.3\times10^{11}$ W/cm$^2$ for electron energy $E=0.34$ eV. (b) Intensity $I=6.5\times10^{11}$ W/cm$^2$ for electron energy $E=0.12$ eV. The experimental data are from Reichle *et al.* [3].

atomic ion after the atom is ionized by the laser [18,27]. For negative ion targets, there is no long-range Coulomb interaction between the electron and the neutral atom following the detachment of the electron by the laser, thus the fanlike structure is absent in the TDSE results, as shown in Fig. 2(a). Figures 2(a) and 2(b) both show clear MPD peaks. The angular distribution of the lowest MPD peak has a maximum at 90° (even parity), thus the dominant angular momentum quantum number should be even. For atomic targets, the dominant angular momentum of the photoelectrons at low energies can be calculated from the propensity rule given in Chen *et al.* [18]. Since the minimum number of photons needed to remove the electron at the laser intensity used is 16 and that the ground state of H$^-$ is an *s* orbital, Fig. 8 of Chen *et al.* [18] shows that the dominant angular momentum is six, and thus the parity is even, in agreement with the calculated results shown in Fig. 2. Note that the next MPD peak would have odd parity since one more photon is absorbed, as clearly seen from the calculated spectra.

Low-energy photoelectron angular distributions of H$^-$ have been reported by Reichle *et al.* [3] using lasers with $\lambda=2150$ nm ($\hbar\omega=0.576$ eV), pulse duration (FWHM) of 250 fs, at two peak intensities $I=1.3\times10^{11}$ W/cm$^2$ and $I=6.5\times10^{11}$ W/cm$^2$, corresponding to Keldysh parameters of 2.6 and 1.2, respectively. Unlike the previous example, this is in the multiphoton regime. In fact, the first low-energy photoelectron peak can be attributed to two-photon absorption. In Fig. 3 we show the angular distributions for photoelectron energy at 0.34 eV for $I=1.3\times10^{11}$ W/cm$^2$ and at 0.12 eV for $I=6.5\times10^{11}$ W/cm$^2$. We compare the experimental data with SFA1 and with TDSE calculations. Both the SFA1 and the TDSE results agree well with the experimental results [the actual values from SFA1 shown have been scaled to agree with the TDSE results at small angles in (a) and at 90° in (b)]. Note that it appears that the SFA1 results are in better agreement with the experimental data in Fig. 3(a) than the TDSE results. However, the volume effect is not included in our calculations and we considered the agreement satisfactory. Our calculations also showed that the angular distributions are independent of the pulse durations.
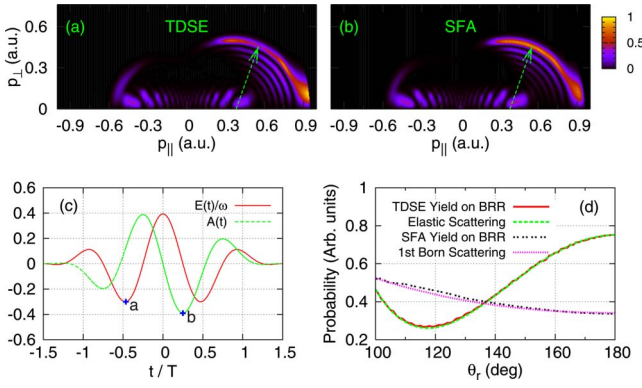
FIG. 4. (Color online) (a),(b) 2D momentum distributions of laser-induced photoelectrons of $H^-$ in the high-energy region, obtained from TDSE and SFA, respectively. The laser parameters are the same as in Fig. 1. (c) The electric field and the vector potential of a three-cycle pulse with the "born time" of the detached electron and its return time indicated. (d) Electron yields along the BRR from the TDSE calculations compared to the electron-H elastic scattering cross sections, and the corresponding results from the SFA compared with the FBA.

Next we return to the laser parameters used in Figs. 1 and 2, and study the 2D momentum distributions of the detached electrons in the high-energy region. It is well known that these high-energy electrons are generated by rescattering processes. In order to highlight these high-energy features, in Figs. 4(a) and 4(b) we show the 2D momentum distributions by renormalizing them such that the total ionization probability density at each energy is the same. The results from the TDSE and from SFA appear to be quite similar globally. Here we focus on the outermost ring of the 2D spectra. The distributions along this ring have been studied for laser-generated photoelectrons from neutral atoms recently [17]. They are called back rescattered ridge (BRR) electrons, representing returning electrons that have been rescattered into the backward directions by the ionized target. The BRR electrons in Fig. 4(a) and 4(b) are electrons that have been rescattered into the backward directions by the neutral atomic hydrogen. In Fig. 4(c), we depict the electric field and the vector potential of a three-cycle laser pulse used in the calculation. Electrons that are released at the half-cycle centered at "a" [see Fig. 4(c)] will return near "b," with peak kinetic energy of $p_r^2/2 = 3.17\bar{U}_p$ where $\bar{U}_p = A_r^2/4$, with $A_r$ being the vector potential at "b." An electron that is scattered into the backward direction with momentum $p_r\hat{\mathbf{p}}_r$ at "b" will gain additional momentum $A_r$ as it emerges from the laser field. Thus the momentum of the BRR electrons at the end of the laser pulse is given by $\mathbf{p} = -\mathbf{A}_r + \mathbf{p}_r$, or $p_\parallel = -A_r - p_r \cos\theta_r$ and $p_\perp = p_r \sin\theta_r$, where $p_r = 1.26A_r$. Here $\theta_r$ is the scattering angle measured from the "incident" direction of the recolliding electrons and for BRR, we consider $\theta_r > 100°$ only. The BRR ring is indicated by an arrow with length from its shifted center shown in Figs. 4(a) and 4(b). In Fig. 4(d) we show the yield of the photoelectrons along the BRR, plotted against the scattering angle $\theta_r$. On the same graph we also show the differential elastic cross sections of electrons scattered by atomic hydrogen. For the laser parameters used in
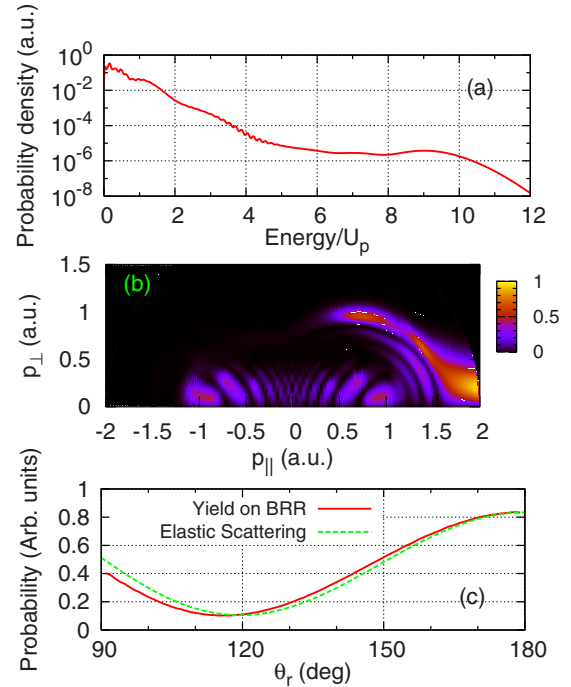


FIG. 5. (Color online) TDSE results for single ionization of $F^-$ in a three-cycle laser pulse with $\lambda = 1800$ nm and $I = 1.3 \times 10^{13}$ W/cm². (a) Energy spectra, (b) 2D electron momentum distributions in the high-energy region, (c) electron yields along the BRR compared to the electron-F elastic scattering cross sections.

this example, $A_r = 0.39$ and thus the electron's kinetic energy is $p_r^2/2 = 3.28$ eV. It can be seen from Fig. 4(d) that the yields along the BRR obtained from the TDSE calculations are in very good agreement with the "exact" electron-hydrogen differential scattering cross sections (normalized). In addition, the yields from the SFA2 calculations are also compared to the differential elastic $e$-H scattering cross sections calculated in the first Born approximation (FBA) and they show good agreement between them as well. The yields along the BRR obtained from the TDSE and SFA2 are clearly different. In particular, the extracted elastic differential cross section from TDSE shows a minimum and becomes larger at large angles. The one extracted from SFA2 or from FBA show that the differential cross sections decrease monotonically with increasing angles. We thus confirm that one can extract differential elastic $e$-H scattering cross sections in the backward directions from laser-induced photodetachment of $H^-$ ions by intense short laser pulses.

We have carried out similar studies for $F^-$ ions, using a three-cycle laser pulse with $\lambda = 1800$ nm and $I = 1.3 \times 10^{13}$ W/cm². The ponderomotive energy $U_p$ is 3.93 eV. In this case, it needs 11 photons to remove the electron from $F^-$. The photoelectron energy spectra and the 2D momentum distributions calculated using TDSE are shown in Figs. 5(a) and 5(b), respectively. It can be seen from Fig. 5(b) that the yields along the BRR show a clear minimum. This minimum is due to the minimum in the differential scattering cross sections between the electrons and neutral fluorine atoms. For the laser parameters used, we calculated that

the returning electron energy is 11.8 eV. In Fig. 5(c) we show the extracted differential scattering cross sections from laser-induced momentum distributions along the BRR, and compare the results with the calculated elastic $e$-F scattering cross sections. The good agreement between the two demonstrates once again that one can extract electron-atom scattering cross sections from laser-induced photoelectron momentum distributions of negative ions.

## IV. SUMMARY AND PERSPECTIVE

In this paper we have studied the photodetachment cross sections of atomic negative ions by an intense laser pulse, using the SFA1+SFA2, and by the TDSE directly. We established that the electron energy spectra and the 2D electron momentum distributions obtained from SFA and from TDSE are quite close to each other. On the other hand, there are important differences in the 2D electron momentum distributions at high energies. These electrons are identified to be distributed along the so-called BRR. From the 2D momentum distributions along the BRR, we have shown that elastic scattering cross sections between free electrons with neutral atom targets can be accurately extracted. In other words, we have shown that specific structure information which has previously been probed with electron scattering can also be obtained from the photodetachment of the negative ions by short intense laser pulses.

The results from this work have two important implications. Since the laser pulses have short durations down to a few femtoseconds, the present results imply that one can probe the time evolution of a transient negative ion system using this method, similar to what one can do with neutral targets [17,28]. Second, it shows that one can extract electron-atom or electron-molecule scattering cross sections by carrying out photodetachment measurements of their negative ions with intense laser pulses. One can control the electron scattering energies by changing laser intensity or wavelength. For many atomic and molecular species, including radicals, it may be easier to produce or control their negative ions than their neutrals. In this case photodetachment of negative ions by intense short laser pulses can potentially offer a much better means for measuring electron scattering cross sections.

Although we have carried out calculations using negative atomic ions treated by a model potential, we believe that our conclusions applies to real many-electron atomic and molecular systems. In fact, it is well-known that electron scattering off an atom or molecule cannot be accurately described using a simple model potential at low incident energies. At present, it is not possible to obtain accurate 2D momentum spectra for many-electron atoms or molecules from TDSE. If accurate laser-generated electron spectra are available, one would expect the data to reveal many-electron effects. For example, in electron-hydrogen atom scattering, in Fig. 4(d) we show that the differential cross section at $E=3.28$ eV has a minimum at 120° according to the model potential we have used. Experimental data by Williams [29] at $E=3.4$ eV indicated that the minimum occurs closer to about 80° (At 8.7 eV the minimum is at about 115°). To achieve agreement for electron scattering at such low energies, more advanced theoretical models which treats both electrons together, such as the Kohn variational principle [30], the polarized orbital method [31] or close-coupling methods [32] are needed. It remains to be seen if laser-induced photoelectron spectra can be measured with high precision such that many-electron effects are revealed. Unlike electron scattering which is a linear phenomenon, laser-induced photoelectron yields are nonlinear phenomena. On the other hand, the present paper shows that the extracted electron scattering cross sections from the BRR are independent of the laser parameters, including their intensity or wavelength (and the duration [22]), so long that the returning electron has the same energy. This may provide an added check on the electron scattering cross sections extracted from laser-induced photoelectron measurements.

[1] D. B. Milošević, G. G. Paulus, D. Bauer, and W. Becker, J. Phys. B **39**, R203 (2006).

[2] P. Agostini and L. F. DiMauro, Rep. Prog. Phys. **67**, 813 (2004).

[3] R. Reichle, H. Helm, and I. Y. Kiyan, Phys. Rev. Lett. **87**, 243001 (2001).

[4] R. Reichle, H. Helm, and I. Y. Kiyan, Phys. Rev. A **68**, 063404 (2003).

[5] I. Y. Kiyan and H. Helm, Phys. Rev. Lett. **90**, 183001 (2003).

[6] B. Bergues, Y. Ni, H. Helm, and I. Y. Kiyan, Phys. Rev. Lett. **95**, 263002 (2005).

[7] B. Bergues, Z. Ansari, D. Hanstorp, and I. Y. Kiyan, Phys. Rev. A **75**, 063415 (2007).

[8] M. V. Frolov, N. L. Manakov, E. A. Pronin, and A. F. Starace, J. Phys. B **36**, L419 (2003).

[9] D. B. Milošević, A. Gazibegovic-Busuladzic, and W. Becker, Phys. Rev. A **68**, 050702(R) (2003).

[10] A. Gazibegovic-Busuladzic, D. B. Milošević, and W. Becker, Phys. Rev. A **70**, 053403 (2004).

[11] S. Bivona, G. Bonanno, R. Burlon, and C. Leone, Phys. Rev. A

**76**, 021401(R) (2007).

[12] H. R. Reiss, Phys. Rev. A **76**, 033404 (2007).

[13] M. V. Frolov, N. L. Manakov, E. A. Pronin, and A. F. Starace, Phys. Rev. Lett. **91**, 053003 (2003).

[14] K. Krajewska, I. I. Fabrikant, and A. F. Starace, Phys. Rev. A **74**, 053407 (2006).

[15] C. Arendt, D. Dimitrovski, and J. S. Briggs, Phys. Rev. A **76**, 023423 (2007).

[16] C. C. Chirila and R. M. Potvliege, Phys. Rev. A **71**, 021402(R) (2005).

[17] T. Morishita, A. T. Le, Z. Chen, and C. D. Lin, Phys. Rev. Lett. **100**, 013903 (2008).

[18] Z. Chen, T. Morishita, A. T. Le, M. Wickenhauser, X. M. Tong, and C. D. Lin, Phys. Rev. A **74**, 053405 (2006).

[19] T. Morishita, Z. Chen, S. Watanabe, and C. D. Lin, Phys. Rev. A **75**, 023407 (2007).

[20] A. Lohr, M. Kleber, R. Kopold, and W. Becker, Phys. Rev. A **55**, R4003 (1997).

[21] D. B. Milošević and F. Ehlotzky, Phys. Rev. A **58**, 3124 (1998).

[22] Z. Chen, T. Morishita, A. T. Le, and C. D. Lin, Phys. Rev. A **76**, 043402 (2007).

[23] M. Lewenstein, K. C. Kulander, K. J. Schafer, and P. H. Bucksbaum, Phys. Rev. A **51**, 1495 (1995).

[24] C. Laughlin and Shih-I. Chu, Phys. Rev. A **48**, 4654 (1993).

[25] C. M. Maharjan, A. S. Alnaser, I. Litvinyuk, P. Ranitovic, and C. L. Cocke, J. Phys. B **39**, 1955 (2006).

[26] A. Rudenko, K. Zrost, C. D. Schröter, V. L. B. de Jesus, B. Feuerstein, R. Moshammer, and J. Ullrich, J. Phys. B **37**, L407 (2004).

[27] D. G. Arbó, S. Yoshida, E. Persson, K. I. Dimitriou, and J. Burgdörfer, Phys. Rev. Lett. **96**, 143003 (2006).

[28] T. Morishita, A. T. Le, Z. Chen, and C. D. Lin, New J. Phys. **10**, 025011 (2008).

[29] J. F. Williams, J. Phys. B **8**, 1683 (1975).

[30] A. Temkin and J. C. Lamkin, Phys. Rev. **121**, 788 (1961).

[31] A. Temkin, Phys. Rev. **126**, 130 (1962).

[32] P. G. Burke, D. F. Gallaher, and S. Geltman, J. Phys. B **2**, 1142 (1969).